

Contents

S1 TanDEM-X data

The TanDEM-X acquisitions and the processed Raw DEMs are reported along with some relevant parameters in Tables S1 and S2 for NPI and SPI, respectively. The footprint of each scene (identified with an unique index within each icefield) is shown in Fig. S1.

S2 SRTM data

The datatakes contributing to the SRTM DEM on the Patagonian icefields are reported in Table S3. The elevation difference of two versions of SRTM (SRTMGL1 and NASADEM) and their differences versus the TanDEM-X global DEM used as reference are shown in Fig. S2. Statistics on stable terrain of the two TDM–SRTM DEM differences are reported in Table S4.

S3 DEM calibration

The absolute calibration of the single DEMs with respect to a reference DEM is performed on selected calibration regions (CRs), some of their features are summarized in Table S5.

S4 Seasonal correction

The average daily SECR measured on the summer 2011/2012 (for three different subsets of glaciers) used to compensate for the missing summer days in the main SECR are plotted versus altitude in Fig. S3. The final correction layers are shown in Fig. S4.

S5 Radar backscatter of TanDEM-X and SRTM

The mosaics of backscatter for the TanDEM-X coverages are shown in Fig. S5. The backscatter mean and standard deviation of the SRTM sub-swaths are shown in Fig. S6.

S6 Uncertainty of SECR and mass balance

The random error rasters for the SECR maps of the two epochs (2000–2012 and 2012–2016) are shown in Fig. S7. Two off-ice semivariograms of the SECR maps (TDM–SRTM and TDM–TDM) are plotted in Fig. S8 and the parameters of the exponential model fit are reported in Table S6. The average values of the systematic error components are reported for all produced SECR maps in Table S7.

S7 Results

A map displaying the obtained average SECR per glacier basin for the two epochs and the average elevation per basin is shown in Fig. S9. The hypsometric curve of the icefield highlighting the distribution of unsurveyed area is given in Fig. S10 and S11 for NPI and SPI, respectively. Hypsometric plots of surface elevation change rate (SECR), volume change rate (VCR) and mass change rate (MCR) for more glaciers than in the main paper are reported in Fig. S12 and S13 for NPI and SPI, respectively. The geodetic mass balance of smaller SPI glaciers is reported in Table S8. The frontal retreat distances and subaqueous volume change estimates for SPI glaciers during the period 2000–2011/2012 are given in Table S9.

S8 Comparison of volume change rate estimates of NPI and SPI

A comparison of our results with published volume change rate results of NPI and SPI based on remote sensing data is given in Table S10. A comparison of our 2012–2016 volume change rates with the results of Foresta et al. (2018) for the glacier basins and glacier subsets they use is given in Table S11.

References

S1 TanDEM-X data

Table S1. Specifications of the TanDEM-X Raw DEMs processed over NPI. Here two full coverages were achieved in summer 2012 (May 2011 on the termini of the western glaciers) and in December 2015. The acquisition time is approximately 6:02 (local time) (UTC–4h). DT: datatake; D: descending orbit; HoA: height of ambiguity; Look ang.: mid-range look angle. Posting long.: posting in longitude in arcsec; the posting in latitude is always 0.4 arcsec. The footprint of each scene within the mosaic, identified through an index, is shown in the maps of Fig. S1. * Experimental acquisitions, not part of the TanDEM-X mission operational plan.

DT ID	Acquisition date	Length [km]	Rel. orbit / direction	Beam	Look ang. [°]	HoA [m]	Posting long. ["]	Scene index
1020455	28/05/2011	93	35 / D	A1 050	40.6	48.4	0.4	1
1058596	05/02/2012	149	35 / D	A1 040	38.4	89.8	0.4	2
1057982	16/02/2012	142	35 / D	A1 030	36.1	89.7	0.4	3
1327457*	03/12/2015	91	35 / D	strip 012	41.0	59.0	0.4	4
1327455*	14/12/2015	146	35 / D	strip 011	39.2	56.0	0.4	5
1327456*	08/12/2015	146	111 / D	strip 004	23.9	33.4	0.4	6
1327454*	19/12/2015	115	111 / D	strip 003	21.4	31.0	0.4	7

Table S2. Specifications of the TanDEM-X Raw DEMs processed over SPI. Here two full coverages were achieved in summer 2012 and in December 2015. A further partial coverage was achieved in December 2011. The acquisition time is between 5:54 and 6:03 (local time) (UTC–4h). DT: datatake; D: descending orbit; HoA: height of ambiguity; Look ang.: mid-range look angle. Posting long.: posting in longitude in arcsec; the posting in latitude is always 0.4 arcsec. The footprint of each scene within the mosaic, identified through an index, is shown in the maps of Fig. S1. * Experimental acquisitions, not part of the TanDEM-X mission operational plan.

DT ID	Acquisition date	Length [km]	Rel. orbit / direction	Beam	Look ang. [°]	HoA [m]	Posting long. ["]	Scene index
1057982	16/02/2012	136	35 / D	A1 030	36.1	88.8	0.4	1
1057647	22/02/2012	102	126 / D	A1 080	46.2	119.4	0.4	2
1057028	04/03/2012	200	126 / D	A1 070	44.5	112.2	0.4	3
1055763	26/03/2012	146; 178	126 / D	A1 060	42.6	105.7	0.4; 0.4	4; 5
1056403	15/03/2012	157; 107	126 / D	A1 050	40.6	99.6	0.4; 0.6	6; 7
1058868	31/01/2012	164	126 / D	A1 040	38.4	94.0	0.6	8
1327461*	03/12/2015	131	35 / D	strip 009	35.3	49.9	0.4	9
1327453*	09/12/2015	173	126 / D	strip 014	44.4	65.4	0.4	10
1327460*	20/12/2015	193	126 / D	strip 013	42.8	62.9	0.4	11
1327459*	31/12/2015	214	126 / D	strip 012	41.0	59.3	0.4	12
1327458*	03/12/2015	136	35 / D	strip 005	26.4	38.3	0.6	13
1327462*	09/12/2015	151	126 / D	strip 010	37.3	53.6	0.6	14
1041196	18/12/2011	147; 179	126 / D	A1 060	42.6	81.4	0.4; 0.4	16; 17
1041468	07/12/2011	202	126 / D	A1 050	40.6	74.6	0.4	18
1040940	29/12/2011	164	126 / D	A1 040	38.4	70.8	0.6	19

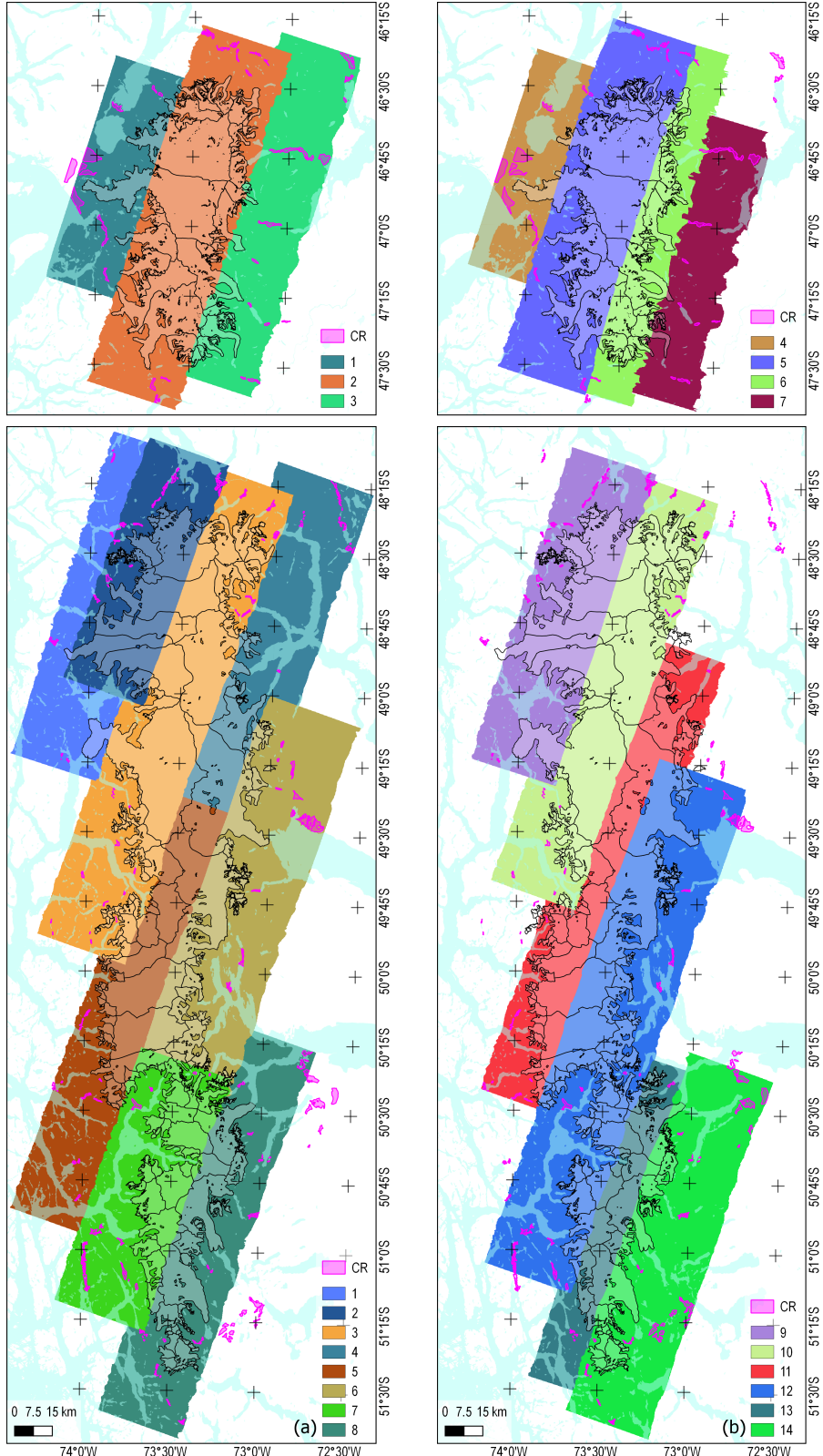


Figure S1. Footprints of the TanDEM-X Raw DEMs forming (a) the 2012 and (b) the 2015 DEM mosaics. The specifications of each Raw DEM, identified by an index, are reported in Tables S1 and S2, for NPI and SPI, respectively. Magenta: the footprints of the calibration regions (CRs) used to perform the DEM coregistration (Sect. 3.1.2).

S2 SRTM data

Table S3. SRTM C-band datatakes covering SPI and NPI. The table reports orbit number, datatake index, orbital direction (A: ascending, D: descending) and the sub-swaths used to compute the average backscattering $\bar{\sigma}^0$ (Sect. 3.2.2). The acquisition time refers to the start of the datatake (Seal and Rogez, 2000).

Orbit n.	DT	Dir.	Sub-swaths	Acq. loc. time (UTC–4h)
10	200	D	4	12/02/2000 04:04
28	230	A	4	13/02/2000 06:56
41	190	D	1	14/02/2000 02:04
44	230	A	3,4	14/02/2000 06:42
57	190	D	1,2	15/02/2000 01:50
60	230	A	2,3,4	15/02/2000 06:29
73	190	D	1,2,3,4	16/02/2000 01:37
76	230	A	1,2,3,4	16/02/2000 06:16
89	190	D	1,2,4	17/02/2000 01:24
92	230	A	1,2,3,4	17/02/2000 06:02
105	200	D	2,3,4	18/02/2000 01:10
108	230	A	2,4	18/02/2000 05:49
121	200	D	1,3,4	19/02/2000 00:57
124	230	A	1,2,3,4	19/02/2000 05:35
137	200	D	1,2,3,4	20/02/2000 00:43
140	230	A	1,2	20/02/2000 05:22
153	200	D	3,4	21/02/2000 00:30
156	240	A	1	21/02/2000 05:09

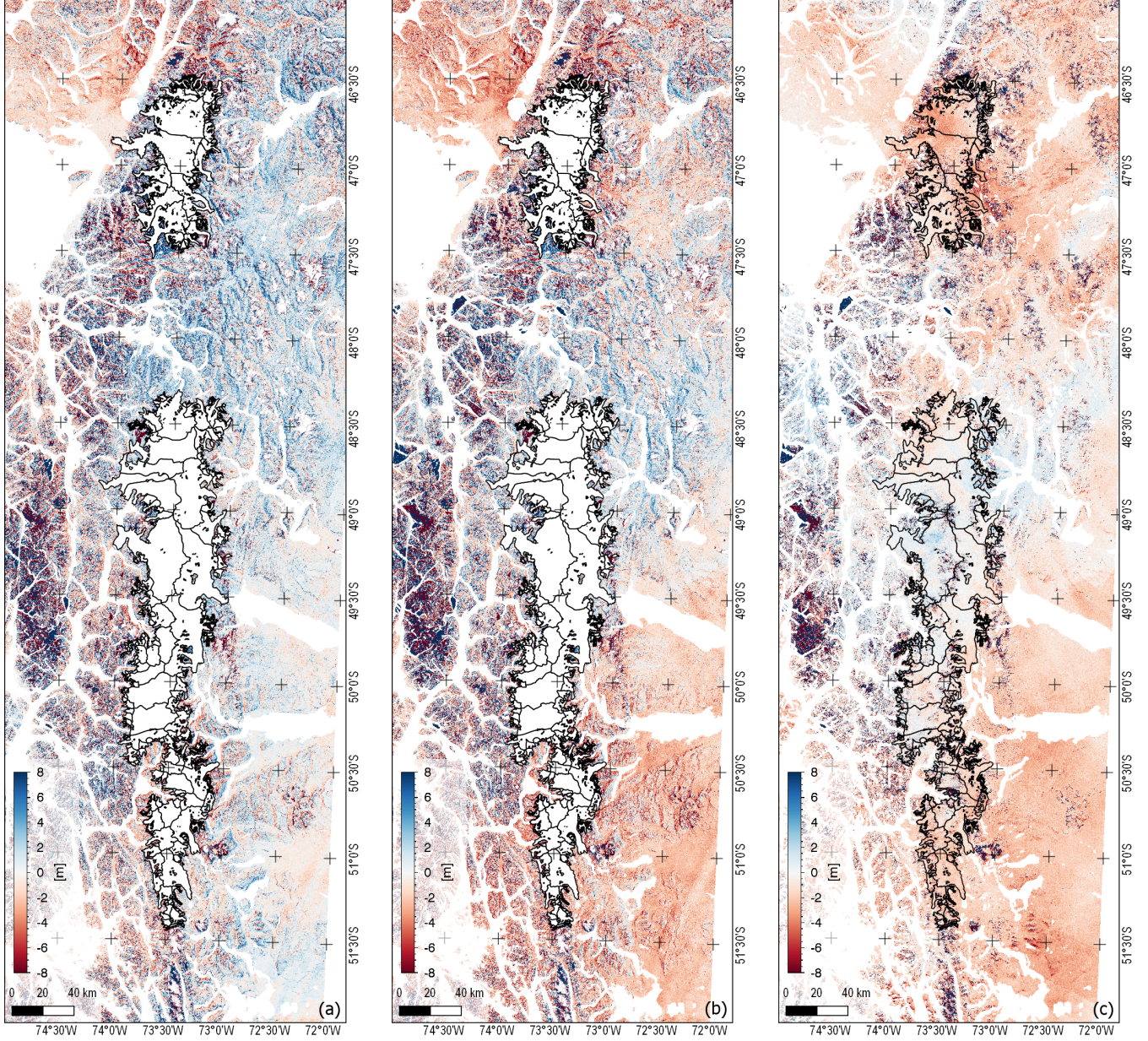


Figure S2. DEM differences at 1 arcsec used to evaluate the two different SRTM data sets. (a) $\Delta h = \text{TDM} - \text{NASADEM}$, (b) $\Delta h = \text{TDM} - \text{SRTMGL1}$ and (c) $\Delta h = \text{NASADEM} - \text{SRTMGL1}$. TDM: TanDEM-X global DEM used as reference elevation (Sect. 3.1.1). The statistics measured on stable terrain on maps (a) and (b) are reported in Table S4.

Table S4. Statistics of the DEM difference between the TDM global DEM and the two SRTM products. The TDM global DEM was scaled to the 1 arcsec posting of the NASADEM and SRTMGL1 DEMs. Approximately 100 million samples were selected on the stable terrain (no ice, no water) visible in Fig. S2, with terrain slope below 40° and a elevation difference $|\Delta h| \leq 20$ m to avoid artefacts (e.g. phase unwrapping errors).

Δh	Mean	Std. dev.	RMS
TDM – NASADEM	0.194 m	3.832 m	3.837 m
TDM – SRTMGL1	-0.982 m	3.895 m	4.017 m

S3 DEM calibration

Table S5. Features of the calibration regions (CRs) selected on stable terrain around NPI and SPI and used to perform DEM coregistration (Sect. 3.1.2).

Reg.	No.	Tot. area	Av. area	Av. elev.	Av. slope
NPI	36	183.8 km ²	5.1 km ²	171.1 m	3.7°
SPI	90	263.8 km ²	2.9 km ²	106.6 m	3.8°

S4 Seasonal correction

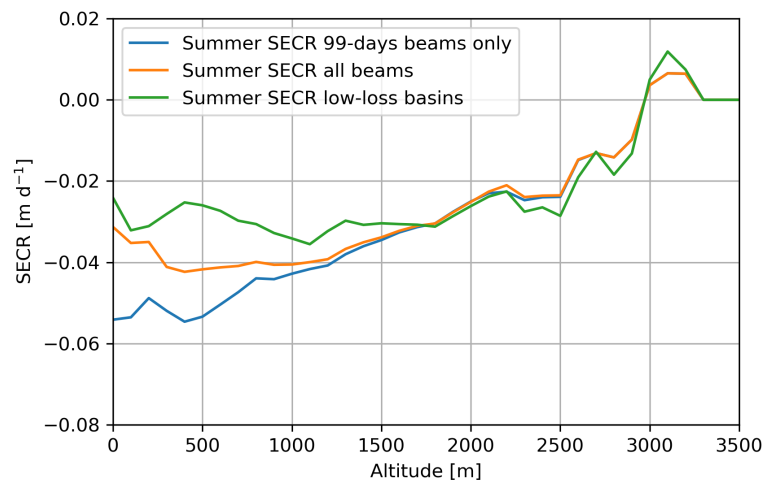


Figure S3. Hypsometric averages extracted from different sub-regions of the summer 2011/2012 SECR (Fig. 8) and used to perform the seasonal correction (Sect. 3.1.3).

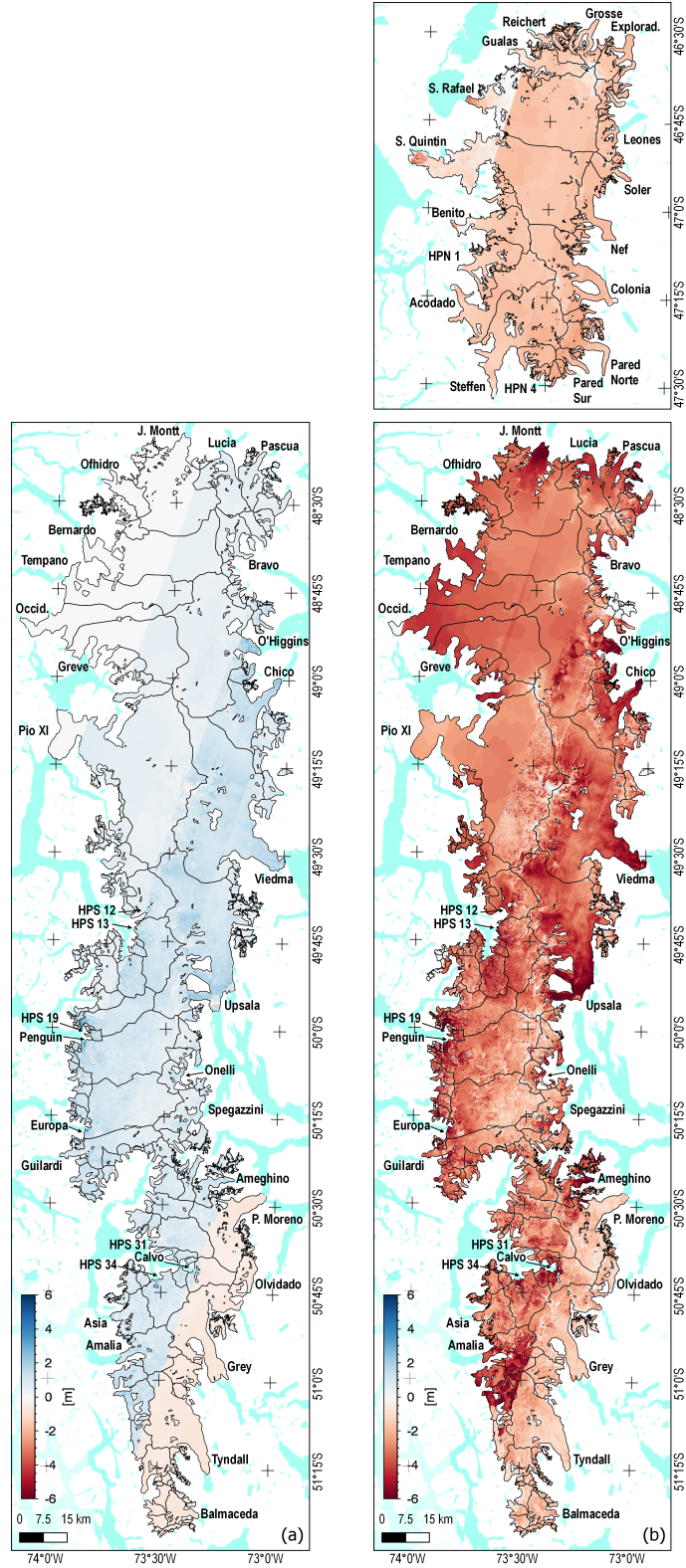


Figure S4. Seasonal correction in metres applied to the SECR maps in order to achieve full temporal coverage for the epochs (a) 2000–2012 and (b) 2012–2016.

S5 Radar backscatter of TanDEM-X and SRTM

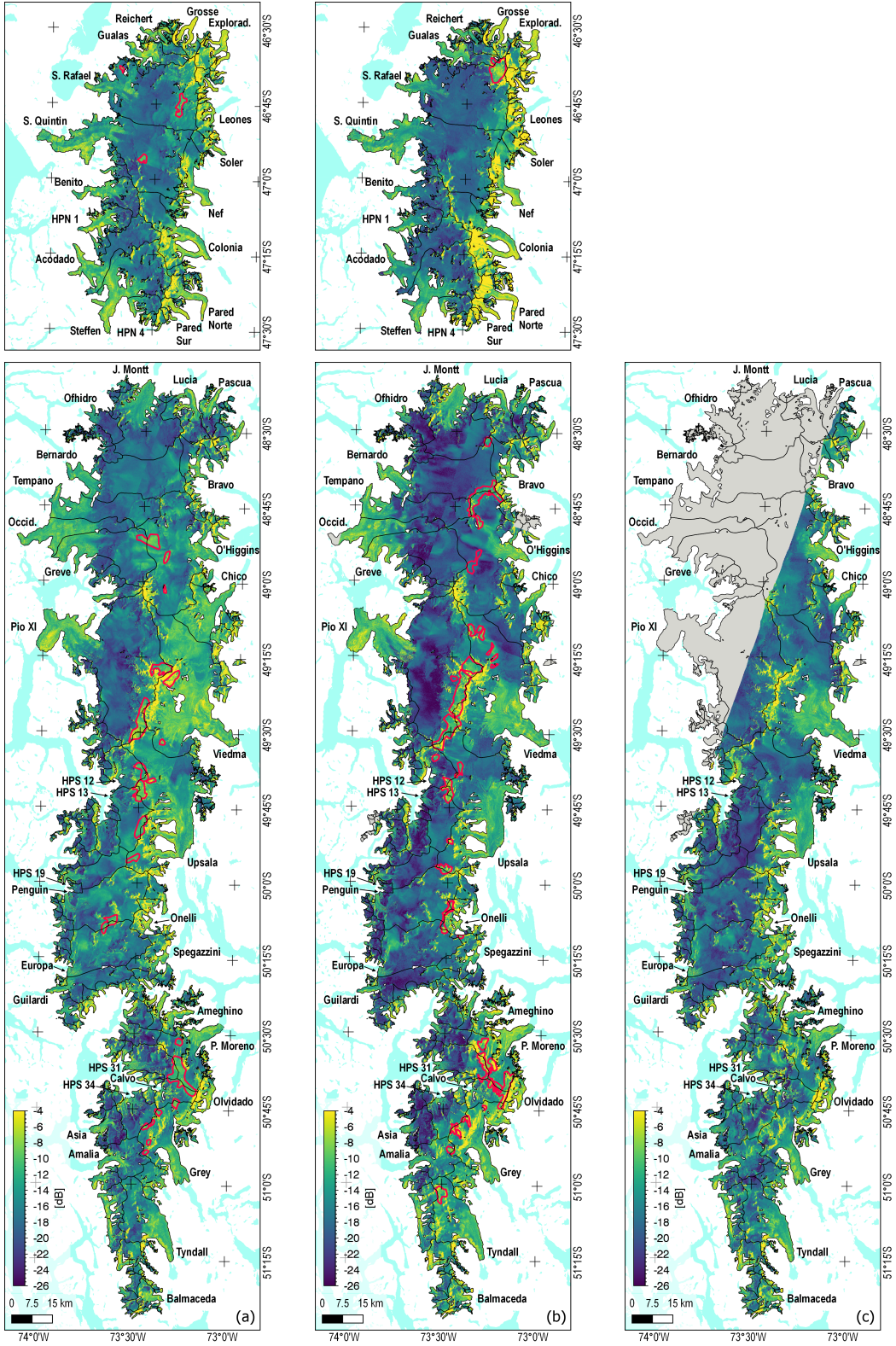


Figure S5. Mosaics of backscattering coefficient σ^0 for all TanDEM-X coverages: (a) Summer 2012, (b) December 2015 and (c) December 2011. Red outlines: regions with high probability of signal penetration, individually taken into account in the error budget. Grey: no coverage.

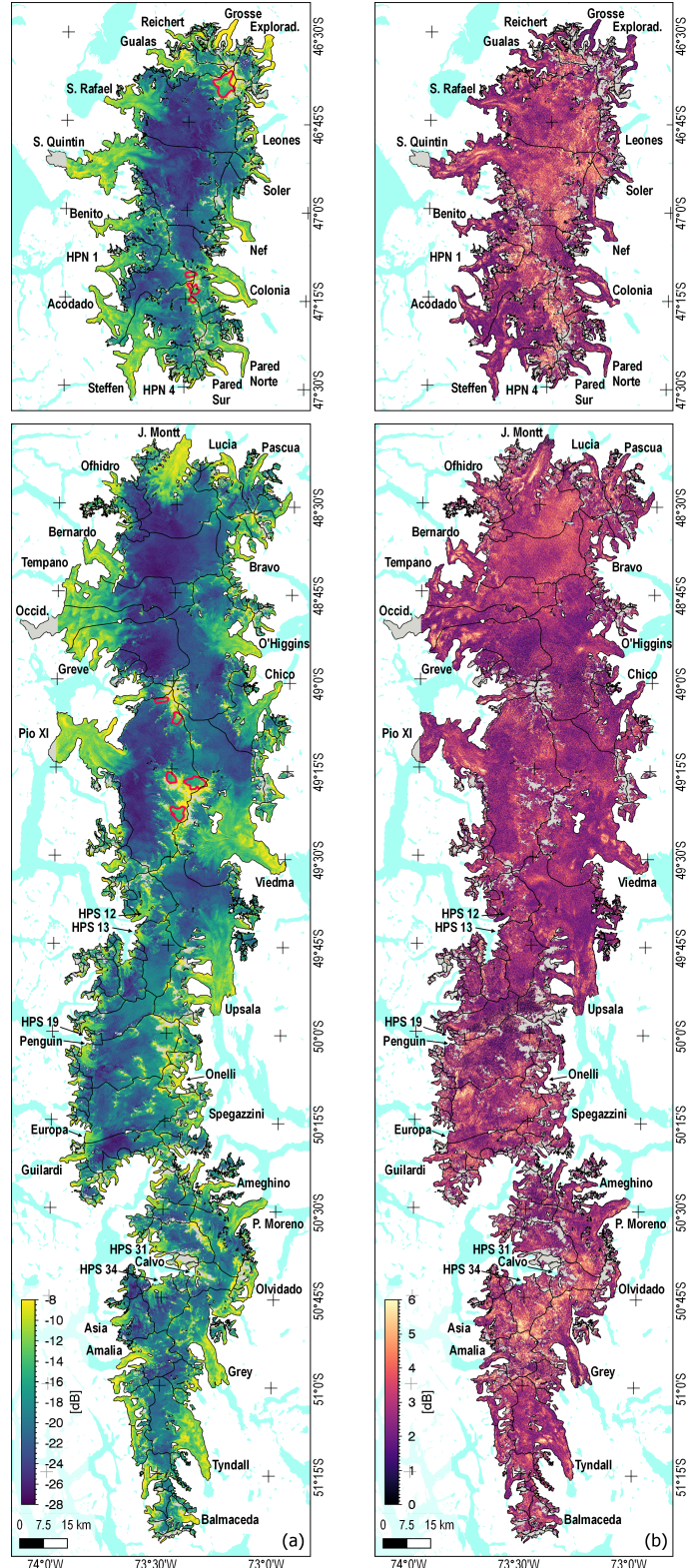


Figure S6. SRTM backscattering (a) mean $\bar{\sigma}^0$ and (b) standard deviation, computed pixelwise on all sub-swaths listed in Table S3. Red outlines: regions with high probability of signal penetration, individually taken into account in the error budget. Grey: no coverage.

S6 Uncertainty of SECR and mass balance

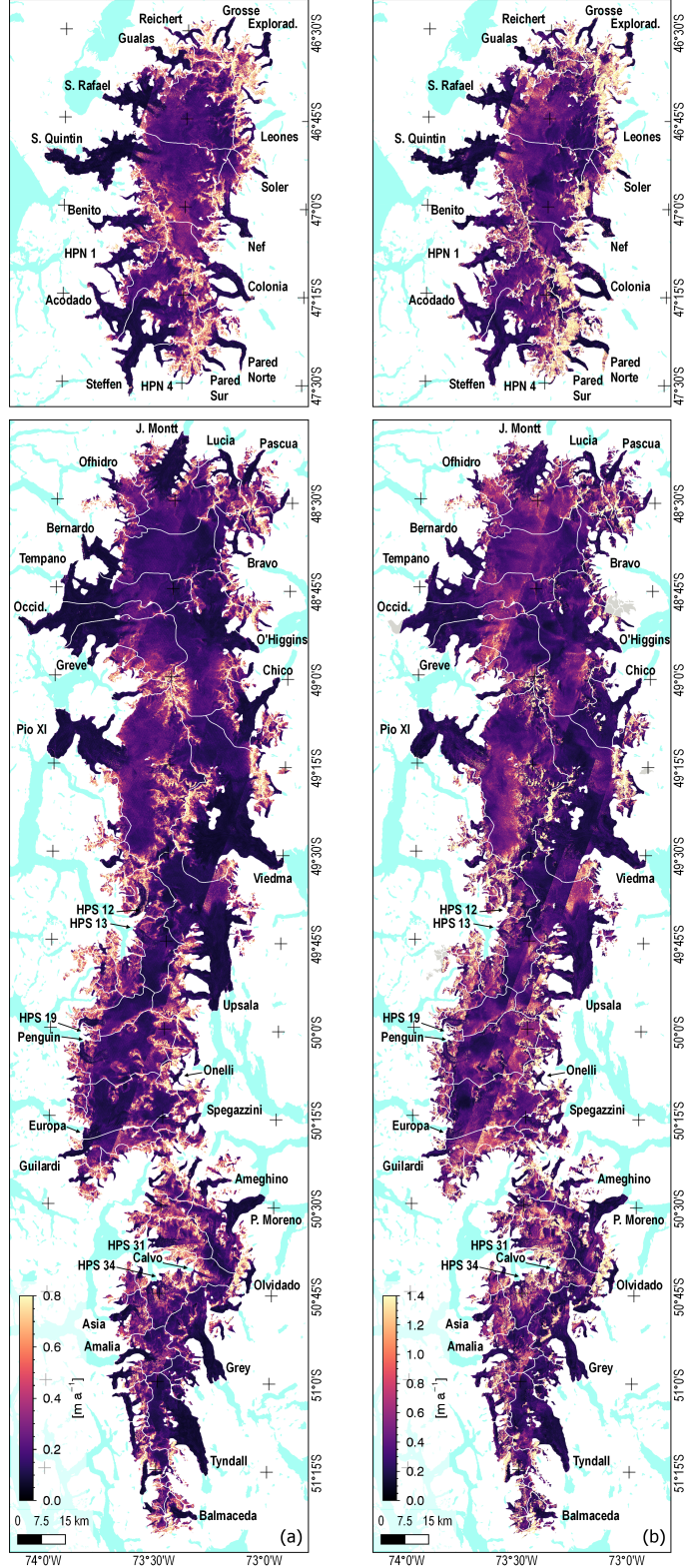


Figure S7. Random error of the SECR maps of (a) 2000–2012 and (b) 2012–2016 obtained as described in Sect. 3.3.1.

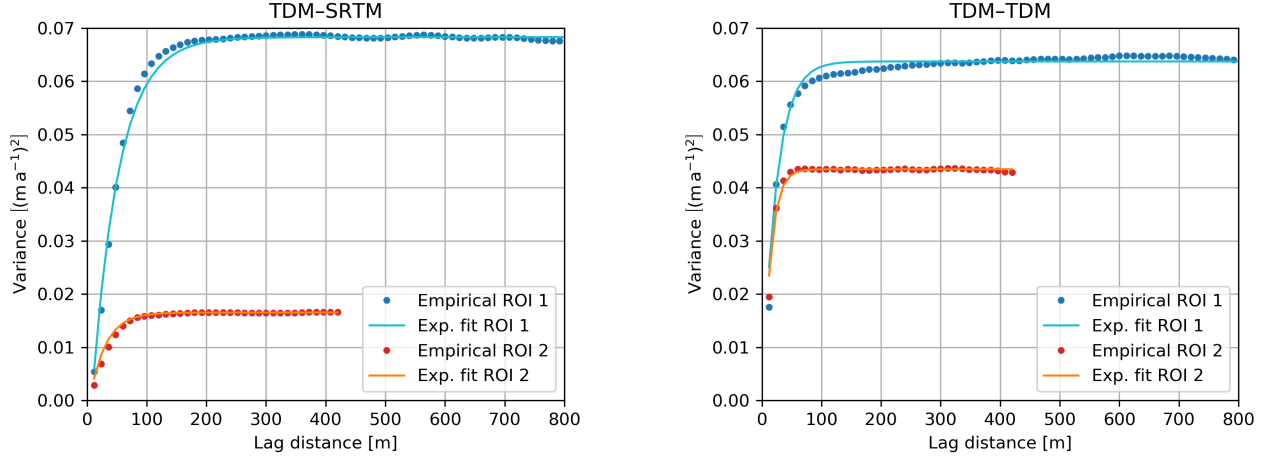


Figure S8. Empirical omnidirectional semivariograms and corresponding exponential model fits computed from a TDM–SRTM SECR and a TDM–TDM SECR for two ice-free regions of interest (ROIs) with different topography (Sect. 3.3.2). ROI 1: hilly terrain with slope distribution similar to the icefields. ROI 2: flat terrain with slope distribution similar to the calibration regions (Sect. 3.1.2). The range, sill and nugget of the fitted exponential semivariogram model are reported in Table S6.

Table S6. Parameters of the exponential semivariogram model fitted to the four empirical semivariograms shown in Fig. S8. The given uncertainties are meant as 1σ .

	Range [m]	Sill $[(\text{ma}^{-1})^2]$	Nugget $[(\text{ma}^{-1})^2]$
ROI 1 TDM–SRTM	135.3 ± 2.8	0.082 ± 0.001	0.013 ± 0.001
ROI 1 TDM–TDM	71.3 ± 3.7	0.064 ± 0.003	0.001 ± 0.003
ROI 2 TDM–SRTM	79.6 ± 5.6	0.019 ± 0.001	0.003 ± 0.001
ROI 2 TDM–TDM	38.5 ± 3.3	0.051 ± 0.005	0.007 ± 0.005

Table S7. Mean of the four systematic error components and mean of the total SECR systematic error computed on the entire icefield for both epochs according to Sect. 3.3.3. ε_{reg} : coregistration error; ε_{pen} : radar signal penetration error; ε_{add} : additional bulk error; $\varepsilon_{\text{seas}}$: seasonal correction error; $\bar{\varepsilon}$: total systematic error.

Data set	Δt [a]	$\overline{\varepsilon}_{\text{reg}}$ $[\text{ma}^{-1}]$	$\overline{\varepsilon}_{\text{pen}}$ $[\text{ma}^{-1}]$	ε_{add} $[\text{ma}^{-1}]$	$\overline{\varepsilon}_{\text{seas}}$ $[\text{ma}^{-1}]$	$\bar{\varepsilon}$ $[\text{ma}^{-1}]$
NPI 2000–2012	12.0	0.0222	0.0127	0.0253	n/a	0.0391
SPI 2000–2012	12.0	0.0169	0.0116	0.0172	0.0088	0.0300
NPI 2012–2016	4.0	0.0590	0.0373	0.0177	0.1185	0.1475
SPI 2012–2016	4.0	0.0514	0.0463	0.0177	0.1043	0.1379

S7 Results

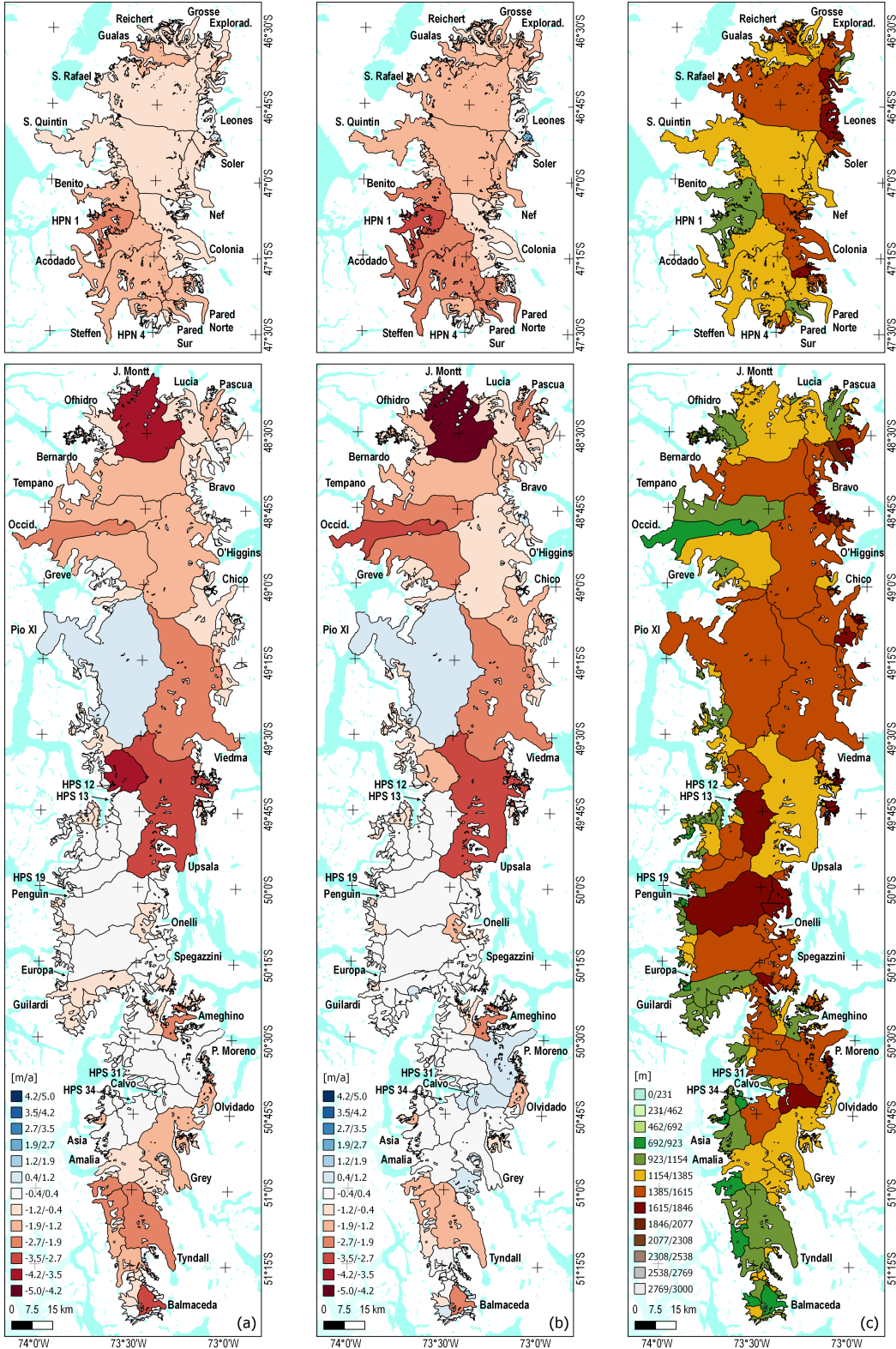


Figure S9. Average SECR per glacier basin of NPI and SPI for the two epochs (a) 2000–2012 and (b) 2012–2016. (c) Average elevation from the TDM 2012 DEM mosaic.

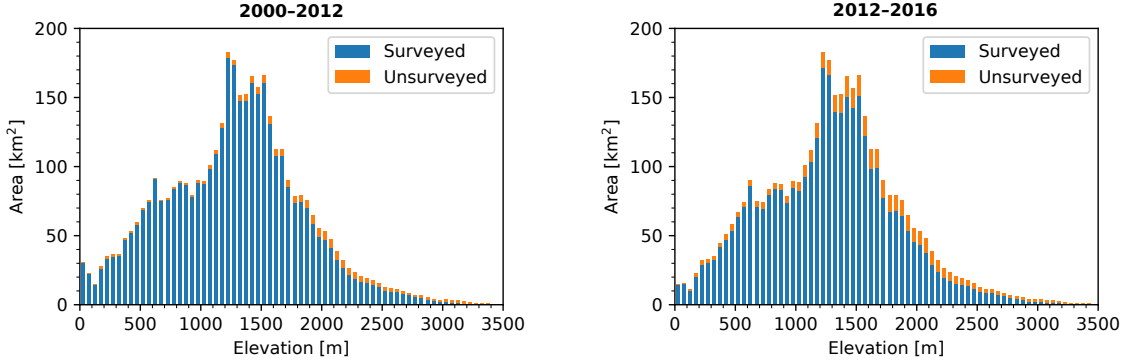


Figure S10. Hypsometry of NPI according to the reference DEM (TDM 2012/2011). The distribution of unsurveyed area in the SECR of 2000–2012 and 2012–2016 is highlighted in orange.

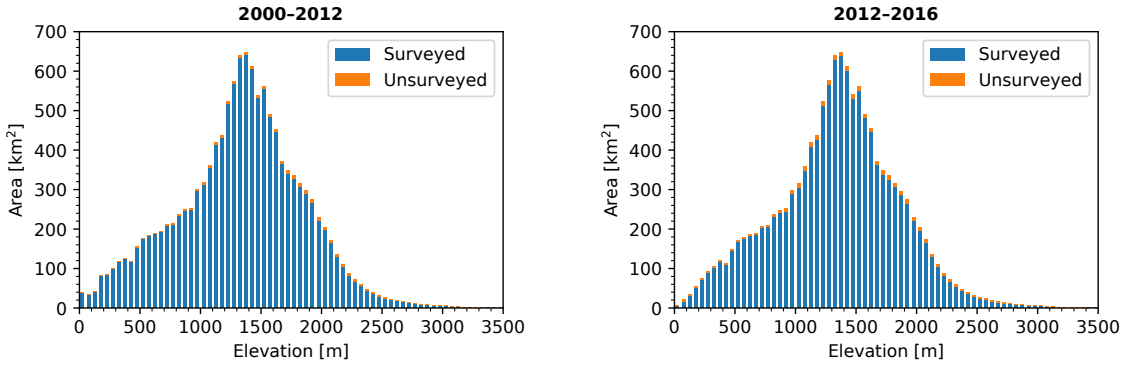


Figure S11. Hypsometry of SPI according to the reference DEM (TDM 2012). The distribution of unsurveyed area in the SECR of 2000–2012 and 2012–2016 is highlighted in orange.

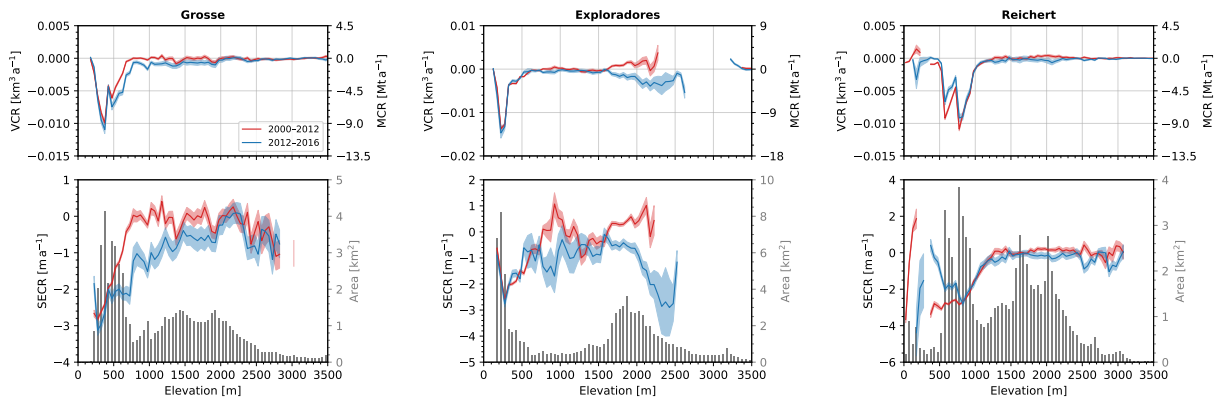


Figure S12. Surface elevation, volume and mass change rates (SECR, VCR, MCR) versus altitude in 50 m intervals for three more glaciers of NPI for epochs 2000–2012 (red) and 2012–2016 (blue). The hypsometric curve of 2012 is shown in grey.

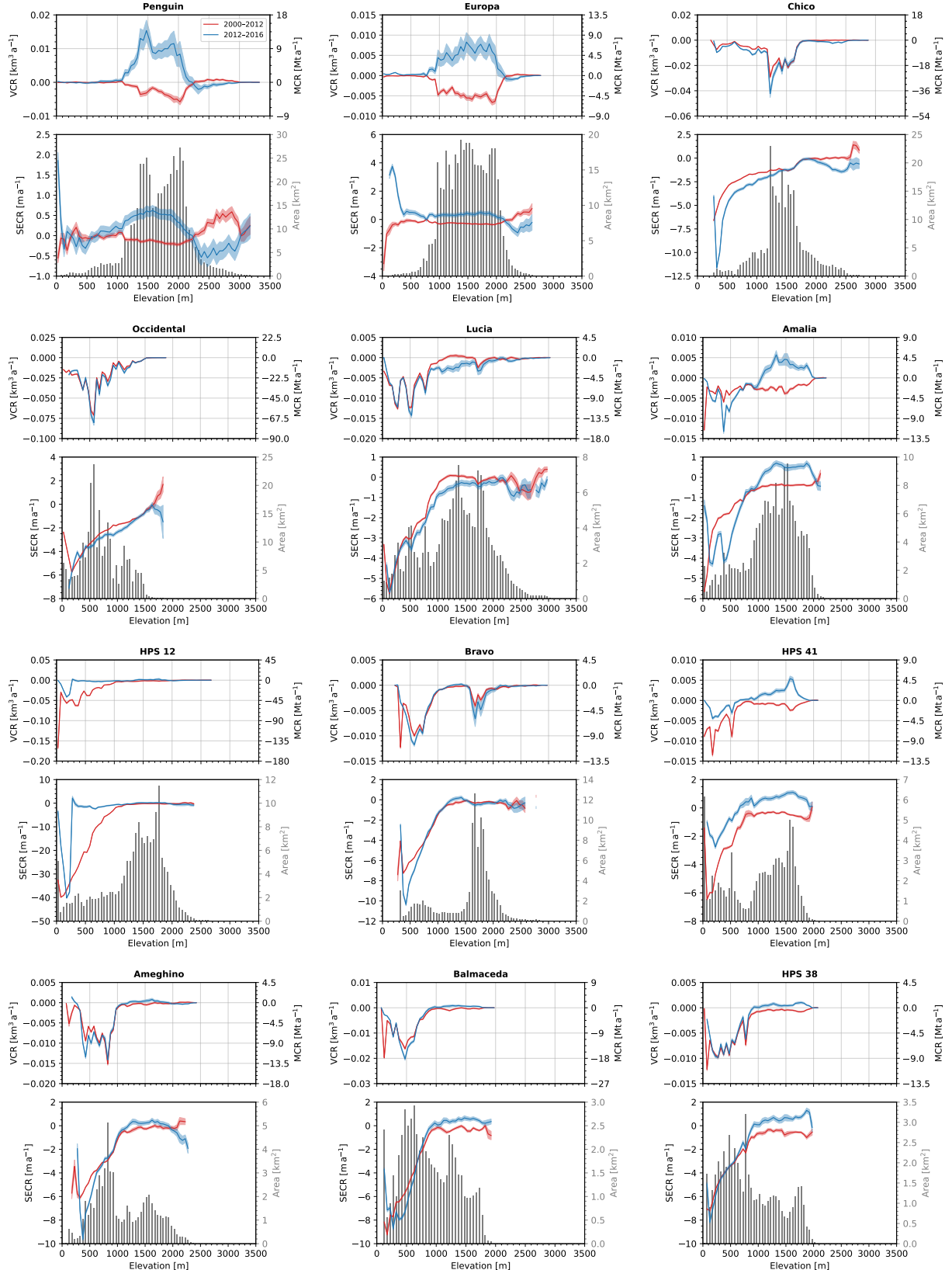


Figure S13. Surface elevation, volume and mass change rates (SECR, VCR, MCR) versus altitude in 50 m intervals for 12 more glaciers of SPI for epochs 2000–2012 (red) and 2012–2016 (blue). The hypsometric curve of 2012 is shown in grey.

Table S8. Average surface elevation change rate (SECR) and volume change rate (VCR) for SPI glaciers smaller than 35 km^2 and larger than 9 km^2 for the two epochs. The reported area refers to the beginning of the epoch, the coverage of the SECR map is also reported. Subaqueous ice changes are not included. The list is continued from Table 3.

RGI Name	2000–2012				2012–2016			
	Area [km 2]	Cov. [%]	Average SECR [ma $^{-1}$]	Volume change [km $^3 \text{ a}^{-1}$]	Area [km 2]	Cov. [%]	Average SECR [ma $^{-1}$]	Volume change [km $^3 \text{ a}^{-1}$]
RGI-17.05044	35.8	99.9	0.934 ± 0.034	0.0321 ± 0.0012	34.4	98.3	0.914 ± 0.124	0.0315 ± 0.0043
RGI-17.05796	35.0	100.0	-0.781 ± 0.033	-0.0273 ± 0.0012	33.7	99.8	-0.551 ± 0.123	-0.0186 ± 0.0042
RGI-17.05130	33.5	100.0	-0.600 ± 0.033	-0.0201 ± 0.0011	33.4	99.5	-0.787 ± 0.125	-0.0262 ± 0.0042
RGI-17.04891	32.6	99.4	-0.298 ± 0.033	-0.0097 ± 0.0011	32.4	98.2	-0.085 ± 0.124	-0.0027 ± 0.0040
RGI-17.15796	31.7	100.0	-0.265 ± 0.030	-0.0084 ± 0.0010	31.4	99.9	-0.194 ± 0.122	-0.0061 ± 0.0038
RGI-17.05889	31.8	98.7	-0.408 ± 0.032	-0.0130 ± 0.0010	30.5	98.9	-1.026 ± 0.124	-0.0313 ± 0.0038
Grande del Torre	30.3	84.4	-0.443 ± 0.041	-0.0134 ± 0.0012	30.1	94.1	-0.754 ± 0.130	-0.0227 ± 0.0039
Bolados	30.0	85.6	-0.429 ± 0.039	-0.0129 ± 0.0012	28.9	97.9	-0.210 ± 0.180	-0.0061 ± 0.0052
RGI-17.05835	28.7	88.5	-0.161 ± 0.038	-0.0046 ± 0.0011	28.7	94.2	-0.556 ± 0.131	-0.0159 ± 0.0037
RGI-17.05338	28.6	99.8	-0.754 ± 0.034	-0.0215 ± 0.0010	28.2	99.3	-0.717 ± 0.123	-0.0202 ± 0.0035
Olvidado	27.4	88.0	-1.672 ± 0.051	-0.0459 ± 0.0014	26.7	91.6	-0.960 ± 0.131	-0.0257 ± 0.0035
RGI-17.05549	26.4	99.7	-0.564 ± 0.036	-0.0149 ± 0.0009	26.4	94.9	-0.514 ± 0.127	-0.0136 ± 0.0034
Mayo Norte	25.9	99.9	-0.483 ± 0.034	-0.0125 ± 0.0009	25.9	98.4	0.057 ± 0.125	0.0015 ± 0.0032
RGI-17.04816	24.3	99.8	-0.401 ± 0.031	-0.0098 ± 0.0008	24.3	99.1	0.202 ± 0.122	0.0049 ± 0.0030
RGI-17.04916	24.3	90.4	-0.261 ± 0.035	-0.0063 ± 0.0009	24.3	98.1	0.147 ± 0.126	0.0036 ± 0.0031
RGI-17.04933	21.6	100.0	-0.606 ± 0.034	-0.0131 ± 0.0007	21.6	98.6	-0.393 ± 0.123	-0.0085 ± 0.0027
RGI-17.04905	21.1	100.0	-0.482 ± 0.032	-0.0102 ± 0.0007	21.1	100.0	0.237 ± 0.121	0.0050 ± 0.0026
RGI-17.04879	20.9	97.1	-0.327 ± 0.038	-0.0068 ± 0.0008	20.9	88.6	0.684 ± 0.132	0.0143 ± 0.0027
RGI-17.04926	19.9	98.9	-0.098 ± 0.032	-0.0020 ± 0.0006	19.9	97.9	0.049 ± 0.124	0.0010 ± 0.0025
Snowy	20.1	97.8	-1.027 ± 0.038	-0.0206 ± 0.0008	19.8	97.0	-0.480 ± 0.123	-0.0095 ± 0.0024
RGI-17.04785	19.7	92.9	-0.256 ± 0.036	-0.0050 ± 0.0007	19.7	93.1	0.562 ± 0.128	0.0111 ± 0.0025
Marconi	19.7	82.3	-0.840 ± 0.051	-0.0165 ± 0.0010	19.4	78.3	-1.159 ± 0.147	-0.0225 ± 0.0029
RGI-17.04993	19.4	89.2	-1.030 ± 0.046	-0.0200 ± 0.0009	18.7	81.4	-0.667 ± 0.135	-0.0125 ± 0.0025
Tunel Inferior	18.1	97.2	-0.737 ± 0.039	-0.0133 ± 0.0007	18.1	96.9	-0.668 ± 0.127	-0.0121 ± 0.0023
RGI-17.15792	17.7	99.9	-0.276 ± 0.034	-0.0049 ± 0.0006	17.7	99.9	-0.020 ± 0.122	-0.0004 ± 0.0022
RGI-17.04884	17.0	51.3	-0.380 ± 0.062	-0.0065 ± 0.0011	17.0	60.9	-0.089 ± 0.156	-0.0015 ± 0.0026
RGI-17.04890	16.9	98.6	-0.265 ± 0.037	-0.0045 ± 0.0006	16.9	95.8	0.188 ± 0.126	0.0032 ± 0.0021
RGI-17.05439	16.2	80.2	-0.078 ± 0.048	-0.0013 ± 0.0008	16.2	54.6	-0.478 ± 0.157	-0.0077 ± 0.0025
RGI-17.04995	16.1	72.8	-0.695 ± 0.055	-0.0112 ± 0.0009	16.1	95.9	-0.702 ± 0.133	-0.0113 ± 0.0021
RGI-17.04901	16.1	89.4	-0.200 ± 0.040	-0.0032 ± 0.0006	16.1	93.3	0.083 ± 0.129	0.0013 ± 0.0021
RGI-17.04862	16.1	100.0	-1.202 ± 0.038	-0.0193 ± 0.0006	16.1	98.9	0.072 ± 0.124	0.0012 ± 0.0020
RGI-17.05092	15.7	99.1	0.196 ± 0.042	0.0031 ± 0.0007	15.7	97.6	-0.413 ± 0.126	-0.0065 ± 0.0020
RGI-17.04923	15.7	92.8	-0.065 ± 0.039	-0.0010 ± 0.0006	15.6	95.2	0.034 ± 0.128	0.0005 ± 0.0020
RGI-17.04931	15.5	100.0	-0.277 ± 0.033	-0.0043 ± 0.0005	15.5	98.2	0.048 ± 0.125	0.0007 ± 0.0019
RGI-17.06038	14.8	98.6	-0.269 ± 0.038	-0.0040 ± 0.0006	14.4	94.7	-0.842 ± 0.129	-0.0122 ± 0.0019
RGI-17.04991	14.0	99.8	0.101 ± 0.033	0.0014 ± 0.0005	14.0	98.8	-0.035 ± 0.125	-0.0005 ± 0.0017
RGI-17.04878	13.9	88.5	-0.225 ± 0.045	-0.0031 ± 0.0006	13.9	99.0	-0.022 ± 0.172	-0.0003 ± 0.0024
RGI-17.05028	13.7	87.5	-0.327 ± 0.048	-0.0045 ± 0.0007	13.7	80.0	-0.167 ± 0.140	-0.0023 ± 0.0019
RGI-17.04959	13.2	90.3	0.277 ± 0.052	0.0037 ± 0.0007	13.0	97.5	-0.473 ± 0.134	-0.0062 ± 0.0017
RGI-17.05627	12.9	99.9	-0.037 ± 0.039	-0.0005 ± 0.0005	12.9	99.6	-0.030 ± 0.127	-0.0004 ± 0.0016
RGI-17.04885	12.8	93.6	-0.003 ± 0.047	-0.0000 ± 0.0006	12.8	92.7	-0.199 ± 0.129	-0.0025 ± 0.0017
RGI-17.04910	12.7	99.9	-0.369 ± 0.033	-0.0047 ± 0.0004	12.7	99.9	0.392 ± 0.123	0.0050 ± 0.0016
RGI-17.05024	12.9	99.7	-0.295 ± 0.038	-0.0038 ± 0.0005	12.6	98.9	0.010 ± 0.125	0.0001 ± 0.0016
RGI-17.05059	12.6	99.1	0.170 ± 0.044	0.0021 ± 0.0006	12.6	95.3	-0.570 ± 0.130	-0.0072 ± 0.0016
RGI-17.01019	12.5	63.9	0.536 ± 0.070	0.0067 ± 0.0009	12.5	89.0	0.157 ± 0.149	0.0020 ± 0.0019
RGI-17.15748	12.5	99.9	0.188 ± 0.041	0.0024 ± 0.0005	12.5	99.2	-0.316 ± 0.126	-0.0040 ± 0.0016
RGI-17.04946	12.2	99.9	-0.289 ± 0.036	-0.0035 ± 0.0004	12.1	98.4	-0.127 ± 0.125	-0.0015 ± 0.0015
RGI-17.15738	11.9	90.7	-0.251 ± 0.044	-0.0030 ± 0.0005	11.9	92.2	-0.356 ± 0.133	-0.0042 ± 0.0016
RGI-17.05505	11.6	93.8	0.039 ± 0.046	0.0005 ± 0.0005	11.6	3.4	-1.397 ± 0.320	-0.0163 ± 0.0037
RGI-17.04906	11.2	64.7	2.373 ± 0.055	0.0265 ± 0.0006	11.2	91.5	-0.435 ± 0.147	-0.0049 ± 0.0016
RGI-17.05459	11.0	95.3	-0.165 ± 0.046	-0.0018 ± 0.0005	11.0	0.0		
RGI-17.15779	10.9	99.5	-0.435 ± 0.049	-0.0047 ± 0.0005	10.9	96.2	0.271 ± 0.131	0.0029 ± 0.0014
RGI-17.15797	10.6	100.0	-1.294 ± 0.041	-0.0137 ± 0.0004	10.6	100.0	-1.379 ± 0.125	-0.0146 ± 0.0013
RGI-17.05022	10.3	90.6	-0.185 ± 0.040	-0.0019 ± 0.0004	10.3	82.7	-0.242 ± 0.137	-0.0025 ± 0.0014
RGI-17.05167	9.6	97.3	0.094 ± 0.048	0.0009 ± 0.0005	9.6	96.9	-0.385 ± 0.133	-0.0037 ± 0.0013
RGI-17.06001	9.4	99.5	0.214 ± 0.045	0.0020 ± 0.0004	9.4	95.1	-0.390 ± 0.131	-0.0037 ± 0.0012
Heim	9.6	83.5	-0.375 ± 0.063	-0.0036 ± 0.0006	9.3	93.9	-0.498 ± 0.146	-0.0047 ± 0.0014
RGI-17.05128	9.2	98.9	-0.179 ± 0.047	-0.0016 ± 0.0004	9.1	99.1	-0.359 ± 0.132	-0.0033 ± 0.0012

Table S9. Estimated subaqueous volume changes for SPI glaciers with most significant frontal changes in the period 2000–2011/2012, based on Abdel Jaber (2016). Δt : the time span in years; d_{fr} : glacier retreat at the central part of the front; VC_{sub} : subaqueous ice volume loss. * Glaciers where bathymetric data at the front was available. Following bulk errors were assigned: 20 % for glaciers with bathymetric data, 70 % for HPS 12, 40 % for other glaciers.

Glacier front	Δt [a]	d_{fr} [km]	VC_{sub} [km^3]
Upsala W*	11.2	3.45	-2.800 ± 0.560
Greve	12.0	1.13	-0.813 ± 0.325
Jorge Montt*	11.2	2.36	-0.680 ± 0.136
Occidental	12.0	2.2	-0.671 ± 0.268
HPS 12	11.1	3	-0.655 ± 0.459
HPS 9	12.0	1.13	-0.618 ± 0.247
HPS 8	12.0	2.9	-0.595 ± 0.238
Tyndall*	11.4	1.3	-0.590 ± 0.118
Amalia	11.7	0.6	-0.552 ± 0.221
HPS 41	11.4	1.85	-0.539 ± 0.216
Balmaceda	12.0	1.48	-0.434 ± 0.174
Upsala E	11.2	2.4 / 1.3	-0.339 ± 0.136
Grey	11.4	0.7 / 0 / 0.7	-0.292 ± 0.117
Viedma	11.2	0.82	-0.279 ± 0.112
Onelli & Bolados	12.1	2	-0.267 ± 0.107
O'Higgins	12.1	0.3	-0.174 ± 0.070
HPS 38	11.7	1.37	-0.168 ± 0.067
Lucia	11.2	1	-0.132 ± 0.053
Dickson	12.0	2.33	-0.130 ± 0.052
Bernardo W	12.0	0.7	-0.079 ± 0.032
Ofhidro N	12.0	0.7	-0.071 ± 0.029
Ofhidro S	12.0	1.38	-0.054 ± 0.022
Ameghino*	11.2	0.85	-0.050 ± 0.010
Pio XI N	12.0	0.53	0.369 ± 0.148
Pio XI S	12.0	1.89	2.283 ± 0.913

S8 Comparison of volume change rate estimates of NPI and SPI

Table S10. Overview of volume change rate (VCR) results on NPI, SPI or both icefields. * Mass change rate (MCR) based on gravimetry, converted using $\rho_{\text{ice}} = 900 \text{ kg m}^{-3}$ when VCR not given. * Geodetic MCR re-converted using $\rho_{\text{ice}} = 900 \pm 125 \text{ kg m}^{-3}$ (Foresta, 2018). † “SPOT-SRTM” method; ‡ “ASTER_trend” method (Dussaillant et al., 2018).

Reference	Region	Period	VCR [$\text{km}^3 \text{a}^{-1}$].
Rignot et al. (2003)	NPI	1968/75–2000	-3.2 ± 0.4
Willis et al. (2012a)	NPI	2000–2011	-4.1 ± 0.1
Willis et al. (2012b)	NPI	2000–2011	-4.9 ± 0.3
Abdel Jaber (2016)	NPI	2000–2014	-4.4 ± 0.1
Dussaillant et al. (2018)	NPI	2000–2012	$-4.6 \pm 0.4^{\dagger}$
Dussaillant et al. (2018)	NPI	2000–2012	$-4.7 \pm 0.3^{\ddagger}$
Foresta et al. (2018)	NPI	2011–2017	$-7.5 \pm 0.8^*$
This study	NPI	2000–2012	-4.3 ± 0.2
This study	NPI	2012–2016	-5.6 ± 0.7
Rignot et al. (2003)	SPI	1968/75–2000	-13.5 ± 0.8
Rignot et al. (2003)	SPI	1995–2000	-38.7 ± 4.4
Willis et al. (2012b)	SPI	2000–2012	-21.2 ± 0.5
Abdel Jaber (2016)	SPI	2000–2011/12	-14.6 ± 0.4
Malz et al. (2018)	SPI	2000–2015	-13.2 ± 3.6
Foresta et al. (2018)	SPI	2011–2017	$-16.1 \pm 1.4^*$
This study	SPI	2000–2012	-14.9 ± 0.5
This study	SPI	2012–2016	-11.9 ± 1.9
Chen et al. (2007)	NPI+SPI	2001–2006	$-27.9 \pm 11.0^*$
Ivins et al. (2011)	NPI+SPI	2003–2009	$-28.9 \pm 6.7^*$
Jacob et al. (2012)	Patagonia	2003–2010	$-25.6 \pm 10.0^*$
Willis et al. (2012b)	NPI+SPI	2000–2011/12	-26.1 ± 0.6
Abdel Jaber (2016)	NPI+SPI	2000–2011/12/14	-19.0 ± 0.4
Foresta et al. (2018)	NPI+SPI	2011–2017	$-23.7 \pm 1.6^*$
This study	NPI+SPI	2000–2012	-19.1 ± 0.6
This study	NPI+SPI	2012–2016	-17.5 ± 2.0

Table S11. Comparison of our volume change rate (VCR) results with those of Foresta et al. (2018) for the glaciers and sub-regions defined in their study. We re-converted their reported mass change rates to VCR using $\rho_{\text{ice}} = 900 \pm 125 \text{ kg m}^{-3}$ (Foresta, 2018). The group of glaciers “SPI-G1” includes basins north of Pio XI and Viedma excluding Jorge Montt, “SPI-G2” includes all glaciers west and south of Upsala excluding Grey and Tyndall. Cov. is the percentage of area coverage of the surface elevation change maps.

Region	Foresta et al. (2018) (2011–2017)			This study (2012–2016)		
	Area [km^2]	Cov. [%]	VCR [$\text{km}^3 \text{a}^{-1}$]	Area [km^2]	Cov. [%]	VCR [$\text{km}^3 \text{a}^{-1}$]
NPI	4046.4	45.7	-7.54 ± 0.75	3914.2	89.8	-5.60 ± 0.71
Jorge Montt	474.4	68.0	-2.44 ± 0.25	471.2	98.6	-2.33 ± 0.07
Upsala	863.1	61.3	-2.98 ± 0.16	823.5	99.3	-2.50 ± 0.13
Viedma	992.3	72.7	-2.52 ± 0.19	971.3	98.9	-2.23 ± 0.15
SPI-G1	3570.1	47.4	-5.63 ± 0.40	3667.8	97.1	-5.42 ± 0.52
SPI-G2	4829.5	39.1	-1.84 ± 1.26	4943.8	95.6	-0.04 ± 0.73
Tyndall	332.0	49.9	-0.67 ± 0.13	302.2	98.4	-0.48 ± 0.04
Grey	333.3	54.0	-0.77 ± 0.23	304.4	96.4	-0.07 ± 0.05
Pio XI	1242.6	65.0	0.74 ± 0.31	1246.7	98.5	1.26 ± 0.21
SPI total	12637.2	49.9	-16.11 ± 1.43	12846.8	97.0	-11.86 ± 1.90

References

- Abdel Jaber, W.: Derivation of mass balance and surface velocity of glaciers by means of high resolution synthetic aperture radar: application to the Patagonian Icefields and Antarctica, Dissertation, Technische Universität München, <http://elib.dlr.de/109075/>, 2016.
- Chen, J. L., Wilson, C. R., Tapley, B. D., Blankenship, D. D., and Ivins, E. R.: Patagonia icefield melting observed by gravity recovery and climate experiment (GRACE), *Geophysical Research Letters*, 34, 2007.
- Dussaillant, I., Berthier, E., and Brun, F.: Geodetic Mass Balance of the Northern Patagonian Icefield from 2000 to 2012 using two independent methods, *Frontiers in Earth Science*, 6, 8, 2018.
- Forestal, L., Gourmelen, N., Weissgerber, F., Nienow, P., Williams, J., Shepherd, A., Drinkwater, M., and Plummer, S.: Heterogeneous and rapid ice loss over the Patagonian Ice Fields revealed by CryoSat-2 swath radar altimetry, *Remote Sensing of Environment*, 211, 441–455, 2018.
- Forestal, L. U.: Applications of CryoSat-2 swath radar altimetry over Icelandic ice caps and Patagonian ice fields, Ph.D. thesis, The University of Edinburgh, 2018.
- Ivins, E. R., Watkins, M. M., Yuan, D.-N., Dietrich, R., Casassa, G., and Rölke, A.: On-land ice loss and glacial isostatic adjustment at the Drake Passage: 2003–2009, *Journal of Geophysical Research: Solid Earth*, 116, <https://doi.org/10.1029/2010JB007607>, 2011.
- Jacob, T., Wahr, J., Pfeffer, W. T., and Swenson, S.: Recent contributions of glaciers and ice caps to sea level rise, *Nature*, 482, 514–518, 2012.
- Malz, P., Meier, W., Casassa, G., Jaña, R., Skvarca, P., and Braun, M. H.: Elevation and mass changes of the Southern Patagonia Icefield derived from TanDEM-X and SRTM Data, *Remote Sensing*, 10, 188, 2018.
- Rignot, E., Rivera, A., and Casassa, G.: Contribution of the Patagonia Icefields of South America to sea level rise, *Science*, 302, 434–437, 2003.
- Seal, D. and Rogez, F.: SRTM As-Flown Mission Timeline, Tech. rep., JPL NASA, http://www2.jpl.nasa.gov/srtm/SRTM_TIM_AF.pdf, 2000.
- Willis, M. J., Melkonian, A. K., Pritchard, M. E., and Ramage, J. M.: Ice loss rates at the Northern Patagonian Icefield derived using a decade of satellite remote sensing, *Remote Sensing of Environment*, 117, 184–198, 2012a.
- Willis, M. J., Melkonian, A. K., Pritchard, M. E., and Rivera, A.: Ice loss from the Southern Patagonian Ice Field, South America, between 2000 and 2012, *Geophysical Research Letters*, 39, 2012b.